Saturation effects in forward-forward dijet production in p + Pb collisions

A. van Hameren,[1] P. Kotko,[1] K. Kutak,[1] C. Marquet,[2] and S. Sapeta[3]

[1]*The H. Niewodniczański Institute of Nuclear Physics PAN, Radzikowskiego 152, 31-342 Kraków, Poland*
[2]*Centre de Physique Théorique, École Polytechnique,CNRS, 91128 Palaiseau, France*
[3]*CERN PH-TH, CH-1211, Geneva 23, Switzerland*

We study saturation effects in the production of forward dijets in proton-lead collisions at the Large Hadron Collider, using the framework of High Energy Factorization. Such configurations, with both jets produced in the forward direction, probe the gluon density of the lead nucleus at a small longitudinal momentum fraction and also limit the phase space for emissions of additional jets. We find significant suppression of the forward dijet azimuthal correlations in proton-lead versus proton-proton collisions, which we attribute to stronger saturation of the gluon density in the nucleus than in the proton. In order to minimize model dependence of our predictions, we use two different extensions of the Balitsky-Kovchegov equation for evolution of the gluon density with subleading corrections.

I. INTRODUCTION

The production of hadronic final states at the Large Hadron Collider (LHC) offers unprecedented opportunities to test parton densities in various kinematic regions. Of particular interest is the forward region, where it is possible to construct hadronic observables that allow us to probe parton densities of one of the colliding hadrons at longitudinal fractions $x \sim 10^{-5}$. At such low values of x, on theoretical grounds, one expects "low-x" effects to be relevant, in particular the phenomenon of gluon saturation [1].

In QCD, saturation is described by nonlinear evolution equations for the gluon density, which resum a subset of diagrams generating contributions of the form $\alpha_s \ln 1/x$. The solutions of small-x evolution equations, together with suitable initial conditions, provide parton densities, which then need to be convoluted with appropriate hard matrix elements in order to obtain predictions for measurable cross sections. The Color Glass Condensate (CGC) (see [2] and references therein) and High Energy Factorization (HEF) [3] are two QCD-based frameworks which can be used for phenomenological studies.

The CGC approach has been very successful in describing forward dihadron production at RHIC [4–6]; in particular, it predicted the suppression of azimuthal correlations in d + Au collisions compared to p + p collisions [7], which was observed later experimentally [8,9]. It has now become necessary to extend the validity of the CGC predictions from RHIC kinematics to the LHC. There, the relevant observables involve high-p_t jets, as opposed to individual hadrons with p_t of the order of a few GeV at RHIC. Furthermore, the advantage of jet observables as compared to hadrons is that they are less sensitive to large uncertainties from fragmentation functions.

In order to accommodate this, the theoretical basis developed in the context of RHIC collisions to compute dihadron correlations must be supplemented with further QCD dynamics, relevant at high p_t. This includes, for instance, coherence in the QCD evolution of the gluon density. However, after accounting for higher order corrections, it was recently argued that the CGC approach to forward particle production may, at the moment, be only under control at low transverse momentum $p_t \leq Q_s$, where Q_s denotes the saturation scale, which precisely signals the onset of parton saturation. There are conflicting results on this matter [10,11], and before this formulation can be used to perform forward jet studies at the LHC, further progress on the theoretical side is needed to clarify the situation.

In view of these potential limitations, we instead investigate forward dijets at the LHC using a different, more practical HEF framework. That framework was recently used to study the forward-central dijet [12,13] configuration [14–17] and trijet production for forward-central and purely forward configuration [18]. In this paper, we employ it to study the forward-forward configuration, which offers some practical advantages. First, that configuration is less demanding theoretically than the central-forward one since the phase space for production of an additional third jet becomes limited. In addition, lower values of x can be accessed, enhancing the sensitivity to saturation effects.

In the context of the LHC, we consider forward dijet production in p + Pb and p + p collisions. Comparisons of p + Pb and p + p cross sections for the same observables can provide some evidences for parton saturation since such effects are further enhanced by increasing the atomic number of one of the colliding particles. In order to make an extensive study of saturation effects in forward-forward dijet systems, we use gluon densities obtained from two different extensions of the original Balitsky-Kovchegov equation [19,20]. The first one incorporates the running of the QCD coupling [21,22], and the second one also includes nonsingular pieces (at low x) of the Dokshitzer-Gribov-Lipatov-Altarelli-Parisi

(DGLAP) splitting function, a sea-quark contribution, and resums dominant corrections from higher orders via a kinematic constraint [23,24].

The paper is organized as follows. In Sec. II, we review the similarities and differences between the CGC and HEF approaches to forward particle production. In Sec. III, we introduce the two evolution scenarios that we consider for the small-x nonlinear evolution of the gluon distribution. In Sec. IV, we present our results for forward dijet production in p + p collisions at the LHC, as well as nuclear modification factors R_{pA} for p + Pb collisions. Finally, Sec. V is devoted to summary.

II. COLOR GLASS CONDENSATE VERSUS HEF

In this section, we recall the CGC description of single- and double-inclusive forward particle production in p + p (and p + A) collisions. We outline the present limitations of that formalism when applied to high-p_t jets and introduce the HEF framework as a viable practical alternative to obtain LHC predictions that include saturation effects.

A. Forward particle production in the CGC

In p + A (or p + p) collisions, particle production at forward rapidities is sensitive to large-x partons from the proton, while the target nucleus (or the other proton) is probed deep in the small-x regime. To compute cross sections in such an asymmetric situation, the appropriate formulation is the so-called hybrid factorization [25], rather than the symmetric k_t factorization adequate for midrapidity observables.

In the hybrid formalism, the large-x partons are described in terms of the usual parton distribution functions of collinear factorization $f_{i/p}$, with a scale dependence given by DGLAP evolution equations, while the small-x gluons of the nucleus are described by transverse momentum-dependent distributions, which evolve toward small x according to nonlinear equations. At leading order, single-inclusive hadron production is given by the following convolution of parton level cross sections with fragmentation functions $D_{h/i}$:

$$\frac{d\sigma^{pA\to hX}}{dyd^2p_t} = \int_{x_F}^1 \frac{dz}{z^2}\left[\sum_q x_1 f_{q/p}(x_1,\mu^2)\right.$$
$$\times \tilde{N}_F\left(x_2,\frac{p_t}{z}\right)D_{h/q}(z,Q^2)$$
$$\left.+ x_1 f_{g/p}(x_1,\mu^2)\tilde{N}_A\left(x_2,\frac{p_t}{z}\right)D_{h/g}(z,Q^2)\right],$$
$$(2.1)$$

where $x_1 = x_F/z$ and $x_2 = x_1 e^{-2y}$ with $x_F = p_t e^y/\sqrt{s}$. The unintegrated gluon distributions $\tilde{N}_{F,A}$ are obtained from the dipole cross section by Fourier transformation:

$$\tilde{N}_{F(A)}(x,k) = \int d^2b \int \frac{d^2r}{(2\pi)^2}e^{-i\mathbf{k}\cdot\mathbf{r}}[1 - N_{F(A)}(x,r,\mathbf{b})],$$
$$(2.2)$$

where $N_{F(A)}(x,r,\mathbf{b})$ is the imaginary part of the scattering amplitude of a fundamental (or adjoint) dipole of transverse size r off the nucleus, at impact parameter $\mathbf{b}$.

This leading-order formula underlies a $2 \to 1$ partonic subprocess and therefore cannot be matched onto standard perturbative results at high p_t. In order to accomplish that, next-to-leading order (NLO) corrections based on $2 \to 2$ kinematics are needed. Formally subleading in the saturation region, some of these corrections become leading in the high-p_t regime, as explained in [26], where it was first realized that NLO corrections are crucial to bring the hybrid formulation of particle production into agreement with the standard perturbative result at large transverse momentum.

Recently, the full NLO corrections to the hybrid formalism have been calculated [27,28]. A first implementation indicates that these corrections are negative at high p_t and in fact dominate over the leading-order result (2.1), leading to a negative cross section [10]. This suggests that calculations beyond NLO accuracy, or performing additional resummations at high p_t, are needed in order to stabilize the perturbative series. By contrast, an alternative work suggests a much simpler solution [11]. It may take some time until a consensus is reached about whether or not the hybrid formalism as it is can be used to perform forward jet studies at the LHC or if it is only under control at low transverse momentum $p_t \lesssim Q_s$.

Interestingly enough, there exists an alternative high-p_t observable which is sensitive to the saturation regime, where the theoretical formulation is under control: nearly back-to-back dijets with a small transverse momentum imbalance $|\mathbf{p_{t1}} + \mathbf{p_{t2}}| \sim Q_s \ll |\mathbf{p_{t1}}|, |\mathbf{p_{t2}}|$. While the general formulation of double-inclusive particle production in the CGC is rather complicated, in this nearly back-to-back situation, the following factorization formula can be derived within the hybrid formalism (in the large-N_c limit) [29,30]:

$$\frac{d\sigma^{pA\to\text{dijets}+X}}{dy_1dy_2d^2p_{1t}d^2p_{2t}}$$
$$= \frac{\alpha_s^2}{(x_1x_2S)^2}\left[\sum_q x_1 f_{q/p}(x_1,\mu^2)\sum_i H_{qg}^{(i)}\mathcal{F}_{qg}^{(i)}(x_2,|\mathbf{p_{1t}}+\mathbf{p_{2t}}|)\right.$$
$$\left.+ \frac{1}{2}x_1 f_{g/p}(x_1,\mu^2)\sum_i H_{gg}^{(i)}\mathcal{F}_{gg}^{(i)}(x_2,|\mathbf{p_{1t}}+\mathbf{p_{2t}}|)\right], \quad (2.3)$$

where the fractions of longitudinal momenta of initial state partons are related to the transverse momenta $p_{1,2t}$ and rapidities $y_{1,2}$ of the final state partons by

$$x_1 = \frac{1}{\sqrt{S}}(p_{1t}e^{y_1} + p_{2t}e^{y_2}),$$

$$x_2 = \frac{1}{\sqrt{S}}(p_{1t}e^{-y_1} + p_{2t}e^{-y_2}), \tag{2.4}$$

and $\sqrt{S}$ is the center of mass energy of the p + A system.

$\mathcal{F}^{(i)}$ and $H^{(i)}$ are various unintegrated gluon distributions and associated hard coefficients, respectively. Their expressions can be found in Refs. [29,30]. In particular, one notes that the different gluon distributions are expressed in terms of only two independent basic ones, the so-called dipole gluon distribution (proportional to $\tilde{N}_F$) and the Weizsäcker-Williams gluon distribution related by Fourier transformation to a quadrupole amplitude and in some approximation to $\tilde{N}_A$. Even though we have in mind the high-p_t jets, we expect that the limitations of this hybrid formalism encountered in the single inclusive case do not have an impact for dijets as long as the imbalance of the system $|\mathbf{p_{t1}} + \mathbf{p_{t2}}|$ does not become larger than Q_s, since this is the argument entering the gluon distributions $\mathcal{F}^{(i)}$.

It is a numerically difficult work to solve the quadrupole evolution equation. Instead, using models for these gluon distributions as opposed to actual QCD evolution equations, formula (2.3) was successfully applied to forward dihadron production at RHIC. However, it was realized later that formula (2.3) must be also supplemented with Sudakov-type factors [31,32] in order to consistently resum the large logarithms that emerge when $Q_s \ll |\mathbf{p_{t1}}|, |\mathbf{p_{t2}}|$.

These are tasks that we leave for future work. In this study, we instead investigate forward dijets using the HEF formalism, which we briefly recall below.

B. The HEF framework

Double-inclusive particle production in the HEF is obtained from the following factorization formula:

$$\frac{d\sigma^{pA \to \text{dijets}+X}}{dy_1 dy_2 d^2 p_{1t} d^2 p_{2t}} = \sum_{a,c,d} \frac{1}{16\pi^3 (x_1 x_2 S)^2}$$
$$\times |\overline{\mathcal{M}_{ag \to cd}}|^2 x_1 f_{a/p}(x_1, \mu^2)$$
$$\times \mathcal{F}_A(x_2, |\mathbf{p_{1t}} + \mathbf{p_{2t}}|) \frac{1}{1 + \delta_{cd}}. \tag{2.5}$$

It is an extension of the collinear-factorization formulation, with a transverse momentum-dependent gluon distribution for the nucleus (or proton in the p + p case) probed at small x. That distribution is simply related to $\tilde{N}_F$ by

$$\mathcal{F}_A(x, k) = \frac{N_c}{\alpha_s(2\pi)^3} \int d^2 b \int d^2 r e^{-i\mathbf{k}\cdot\mathbf{r}} \nabla_r^2 N_F(x, r, \mathbf{b})$$
$$= \frac{N_c k^2}{2\pi\alpha_s} \tilde{N}_F(x, k). \tag{2.6}$$

The quantities $|\overline{\mathcal{M}_{ag \to cd}}|^2$ are $2 \to 2$ polarization-averaged matrix elements with an off-shell small-x gluon. The following partonic subprocesses contribute to the production of the dijet system:

$$qg \to qg, \qquad gg \to q\bar{q}, \qquad gg \to gg. \tag{2.7}$$

In contrast to formula (2.3), the large N_c limit is not assumed here; hence, the $gg \to q\bar{q}$ subprocess is not neglected. The corresponding amplitudes were computed in [12] and cross-checked independently in [33,34] using different methods. The expressions are given in the Appendix.

Finally, let us emphasize that this framework should be considered as a model since, in general, there exists no transverse momentum factorization theorem for jet production in hadron-hadron collisions. Even in the nearly back-to-back limit $|\mathbf{p_{t1}} + \mathbf{p_{t2}}| \ll |\mathbf{p_{t1}}|, |\mathbf{p_{t2}}|$, where the factorization (2.3) could be established for dilute/dense collisions (p + A or forward production), several gluon distributions are involved, which is not the case in (2.5). We do note, however, that there exist a kinematic window, namely $Q_s \ll |\mathbf{p_{t1}} + \mathbf{p_{t2}}| \ll |\mathbf{p_{t1}}|, |\mathbf{p_{t2}}|$, in which that formula can be motivated [35]. Indeed, when $|\mathbf{p_{t1}} + \mathbf{p_{t2}}| \ll |\mathbf{p_{t1}}|, |\mathbf{p_{t2}}|$, the off-shell matrix elements given in the Appendix reduce to those of Eq. (2.3), and when $Q_s \ll |\mathbf{p_{t1}} + \mathbf{p_{t2}}|$, the different gluon distributions of Eq. (2.3) have the same asymptotic behavior as $\tilde{N}_F$. We elaborate on this in a future publication.

III. NONLINEAR EVOLUTION OF THE UNINTEGRATED GLUON DISTRIBUTIONS

In order to complete our formulation of the forward jet cross sections, we discuss now the x evolution of the unintegrated gluon distributions.

A. The rcBK evolution

In the CGC framework, the evolution of $\tilde{N}_F$ is obtained from the evolution of the dipole scattering amplitude $N_F(x, r, \mathbf{b})$ [see (2.2)], with the assumption that the impact parameter dependence of N_F factorizes and therefore does not mix with the evolution.

The evolution equation of the dipole amplitude, known as the Balitsky-Kovchegov equation [19,20], supplemented with running coupling corrections (henceforth referred to as rcBK equation) reads ($r_i = |\mathbf{r_i}|$)

$$\frac{\partial N_F(r,x)}{\partial \ln(x_0/x)} = \int d^2 r_1 K^{\text{run}}(\mathbf{r}, \mathbf{r_1}, \mathbf{r_2})[N_F(r_1, x) + N_F(r_2, x)$$
$$- N_F(r, x) - N_F(r_1, x)N_F(r_2, x)], \tag{3.1}$$

with $\mathbf{r_2} \equiv \mathbf{r} - \mathbf{r_1}$ and where x_0 is some initial value for the evolution (usually chosen to be 0.01). K^{run} is the evolution kernel including running coupling corrections. Different prescriptions have been proposed in the literature for K^{run}.

As shown in [36], Balitsky's prescription minimizes the role of higher *conformal* corrections:

$$K^{\mathrm{run}}(\mathbf{r}, \mathbf{r_1}, \mathbf{r_2}) = \frac{N_c \alpha_s(r^2)}{2\pi^2} \left[\frac{1}{r_1^2} \left(\frac{\alpha_s(r_1^2)}{\alpha_s(r_2^2)} - 1 \right) + \frac{r^2}{r_1^2 r_2^2} + \frac{1}{r_2^2} \left(\frac{\alpha_s(r_2^2)}{\alpha_s(r_1^2)} - 1 \right) \right]. \qquad (3.2)$$

The rcBK evolution is independent of whether the target is a proton or a nucleus. That difference is accounted for in the initial condition. The parametrization usually used is

$$N_F(r, x = x_0) = 1 - \exp\left[-\frac{(r^2 Q_{s0}^2)^\gamma}{4} \ln\left(\frac{1}{\Lambda r} + e \right) \right], \qquad (3.3)$$

where, $\Lambda = 0.241$ GeV, Q_{s0} is the saturation scale at the initial x_0, and γ is a dimensionless parameter that controls the steepness of the unintegrated gluon distribution for momenta above the initial saturation scale $k_t > Q_{s0}$. In the proton case, the free parameters are obtained from a fit [37] to HERA proton structure function data [38]: $\gamma = 1.119$ and $Q_{s0}^2 = 0.168$ GeV^2. In the nucleus case, we use identical parameters except for Q_{s0}^2 for which we use

$$Q_{s0}^{2,A} = d Q_{s0}^2 \qquad (3.4)$$

and vary the d parameter between two and four. We note that the resulting unintegrated gluon distributions $\tilde{N}_F$ are those used in the rcBK Monte Carlo [39].

The corresponding Balitsky-Kovchegov (BK) equation in momentum space, for the unintegrated gluon density $\mathcal{F}$, reads [24,40]:

$$\mathcal{F}_p(x, k^2) = \mathcal{F}_p^{(0)}(x, k^2) + \frac{\alpha_s N_c}{\pi} \int_x^1 \frac{dz}{z} \int_{k_0^2}^\infty \frac{dl^2}{l^2} \left\{ \frac{l^2 \mathcal{F}_p(\frac{x}{z}, l^2) - k^2 \mathcal{F}_p(\frac{x}{z}, k^2)}{|l^2 - k^2|} + \frac{k^2 \mathcal{F}_p(\frac{x}{z}, k^2)}{|4l^4 + k^4|^{\frac{1}{2}}} \right\}$$
$$- \frac{2\alpha_s^2}{R^2} \left[\left(\int_{k^2}^\infty \frac{dl^2}{l^2} \mathcal{F}_p(x, l^2) \right)^2 + \mathcal{F}_p(x, k^2) \int_{k^2}^\infty \frac{dl^2}{l^2} \ln\left(\frac{l^2}{k^2} \right) \mathcal{F}_p(x, l^2) \right]. \qquad (3.5)$$

In this formulation one can relatively easily include dominant corrections of higher orders as is discussed in the next section. Note that in order to write the nonlinear term of this equation for the impact-parameter-integrated gluon distribution, we have assumed that the impact parameter integral gives $\int d^2 b = \pi R^2$ where R is a radius of the target proton. The equation for $\mathcal{F}_A$ in the nuclear case is discussed below.

B. The KS gluon density

In principle, the gluon density in the HEF framework $\mathcal{F}_p$ evolves with x according to the Balitsky-Fadin-Kuraev-Lipatov (BFKL) evolution [41]. However, the Ciafaloni-Catani-Fiorani-Marchesini (CCFM) equation [42–44] can also be used to take into account coherence effects in the evolution. The coherence effect in the emissions of gluons is a manifestation of their quantum nature. Its inclusion in the evolution leads to angular ordering of subsequently emitted gluons during evolution. If the newly emitted gluon

violates the imposed ordering, it does not contribute to building up the gluon density. Consequently, emitted gluons which build up the density have to be emitted with increasing angle. The coherence will also introduce a constraint on maximal allowed angle in the evolution of gluons which is linked to the transverse momentum of the measured dijet system.

The BK evolution introduced above can also be used to take into account nonlinear corrections to the BFKL evolution. Both nonlinear and coherence effects can be included simultaneously [45–47], which is in principle required, since we are interested in observables sensitive to both the saturation regime and high-p_t physics. We will be able to do so when the resulting gluon density constrained by HERA data becomes available. So far, only purely theoretical, numerical results are available [48,49].

In the meantime, we use the simplified equation proposed in [24,50]:

$$\mathcal{F}_p(x, k^2) = \mathcal{F}_p^{(0)}(x, k^2) + \frac{\alpha_s(k^2) N_c}{\pi} \int_x^1 \frac{dz}{z} \int_{k_0^2}^\infty \frac{dl^2}{l^2} \left\{ \frac{l^2 \mathcal{F}_p(\frac{x}{z}, l^2) \theta(\frac{k^2}{z} - l^2) - k^2 \mathcal{F}_p(\frac{x}{z}, k^2)}{|l^2 - k^2|} + \frac{k^2 \mathcal{F}_p(\frac{x}{z}, k^2)}{|4l^4 + k^4|^{\frac{1}{2}}} \right\}$$
$$+ \frac{\alpha_s(k^2)}{2\pi k^2} \int_x^1 dz \left[\left(P_{gg}(z) - \frac{2N_c}{z} \right) \int_{k_0^2}^{k^2} dl^2 \mathcal{F}_p\left(\frac{x}{z}, l^2 \right) + z P_{gq}(z) \Sigma\left(\frac{x}{z}, k^2 \right) \right]$$
$$- \frac{2\alpha_s^2(k^2)}{R^2} \left[\left(\int_{k^2}^\infty \frac{dl^2}{l^2} \mathcal{F}_p(x, l^2) \right)^2 + \mathcal{F}_p(x, k^2) \int_{k^2}^\infty \frac{dl^2}{l^2} \ln\left(\frac{l^2}{k^2} \right) \mathcal{F}_p(x, l^2) \right], \qquad (3.6)$$

where $z = x/x'$. This is the BK equation extended to take into account higher order corrections coming from including nonsingular pieces of the gluon splitting function, kinematic constraint effects, and contributions from sea quarks. The input gluon distribution $\mathcal{F}_p^{(0)}(x, k^2)$ is given by

$$\mathcal{F}_p^{(0)}(x, k^2) = \frac{\alpha_S(k^2)}{2\pi k^2} \int_x^1 dz P_{gg}(z) \frac{x}{z} g\left(\frac{x}{z}, k_0^2\right), \quad (3.7)$$

where $xg(x, k_0^2)$ is the integrated gluon distribution at the initial scale, which we set to $k_0^2 = 1 \text{ GeV}^2$. We take the following parametrization:

$$xg(x, 1 \text{ GeV}^2) = N(1-x)^\beta (1 - Dx). \quad (3.8)$$

The parameters N, β, D, together with the proton radius, R, were constrained with a fit to HERA data [38] in [17]; hence, we refer to the resulting gluon density as the Kutak-Sapeta (KS) gluon. The fit gave the following result: $N = 0.994$, $\beta = 18.6$, $D = -82.1$, $R = 2.40 \text{ GeV}^{-1}$.

In order to use Eq. (3.6) to obtain the nuclear gluon density $\mathcal{F}_A$, one needs to make the following formal substitution:

$$\frac{1}{R^2} \to c \frac{A}{R_A^2}, \qquad \text{where} \quad R_A^2 = R^2 A^{2/3}. \quad (3.9)$$

In the above equation, R_A is the nuclear radius, where A is the mass number ($A = 207$ for Pb) and c is a parameter that we vary between 0.5 and 1 to assess the uncertainty related to the nonlinear term. The density $\mathcal{F}_A$ obtained from Eq. (3.6) with the substitution above is the nuclear gluon density normalized to the number of nucleons in the nuclei.

Since the KS evolution equation is already A dependent through the nonlinear term (it has to be so since $\mathcal{F}_A$ is an impact parameter integrated distribution), our prescription for the initial condition is to choose the same in the nuclear case as in the proton case $\mathcal{F}_A^{(0)}(x, k^2) = \mathcal{F}_p^{(0)}(x, k^2)$. This is an interesting difference with the rcBK gluon density (for which it is the initial condition that is A dependent while the evolution equation is A independent), the impact of which we discuss in the following section.

IV. FORWARD-FORWARD DIJET PRODUCTION AT THE LHC

We move now to the numerical results for forward dijet production at the LHC in p + p and p + pb collisions.

Our predictions were generated with the forward region defined as the rapidity range $3.2 < y < 4.9$. The two hardest jets (sorted according to their p_t, $p_{t1} > p_{t2}$) are required to lie within this region. In order to cut off collinear and soft singularities, we use the anti-k_t algorithm [51], with radius $R = 0.5$, and we require each jet to have p_t above 20 GeV. Since, in our modeling, a jet is a single parton, the application of the anti-k_t jet algorithm boils

down to a cut in the $y - \phi$ plane. If the distance between two partons $\Delta R_{ij} = \sqrt{\Delta\phi_{ij}^2 + \Delta y_{ij}^2} > R$, then they form two separate jets; otherwise, they form one jet, and the corresponding event is rejected.

The calculations were performed and cross-checked using three independent Monte Carlo programs: (i) FORWARD [52], which is a direct implementation of Eq. (2.5) and uses the VEGAS algorithm [53,54] for integration, (ii) a program implementing the method of [34] using KALEU [55] and PARNI [56] for integration, and (iii) LXJET [57] using the FOAM program [58] for integration. As mentioned in the previous section, we performed our computations using two different unintegrated gluon distributions, rcBK and KS. For the collinear PDFs, which also enter the HEF formula (2.5), we took the general-purpose CT10 set [59]. For the central value of the factorization and renormalization scale, we chose the average transverse momentum of the two leading jets, $\mu_F = \mu_R = \frac{1}{2}(p_{t1} + p_{t2})$.

Fig. 1 shows the differential cross sections for p + p collision at the center of mass energy of 7 TeV. Two bands come from using two different unintegrated gluons: rcBK and KS. The width of a band corresponds to the renormalization and factorization scale uncertainties obtained by varying the central value by factors 2 and $\frac{1}{2}$. In our framework, scale dependence enters the collinear PDFs and the strong coupling constant, α_s, that resides inside the matrix element. Since our calculation is formally leading order, in terms of powers of α_s, there is nothing to compensate for the scale dependence; thus, the uncertainties for the absolute predictions, shown in Fig. 1, are substantial. They cancel to large extent for the nuclear modification ratios, which we discuss later in this section.

The results with the KS gluon [17] are absolute predictions both in terms of shape and normalization. For the rcBK case, however, since the original gluon density is obtained prior to impact-parameter integration, while the HEF formula (2.5) requires an impact-parameter integrated gluon distribution, there is an ambiguity as to which normalization should be chosen. In the rcBK bands in Fig. 1, we have adjusted the normalization so that it gives a cross section comparable to the KS case, in the range $p_{t1} = 50 - 80$ GeV, a window where the KS predictions reproduce the data well in the central-forward case [17]. We emphasize, however, that when comparing the rcBK and KS distribution, one should concentrate rather on the shape differences. This ambiguity is removed later in this section, when we turn to nuclear modification factors, which are ratios of distribution where the normalization factors cancel.

In the left plot from Fig. 1, we show the distribution of transverse momentum of the leading jet. We see that the differences between KS and rcBK are not only in normalization but also in shape with the latter gluon leading to a steeper p_t spectrum. The middle plot compares rapidity
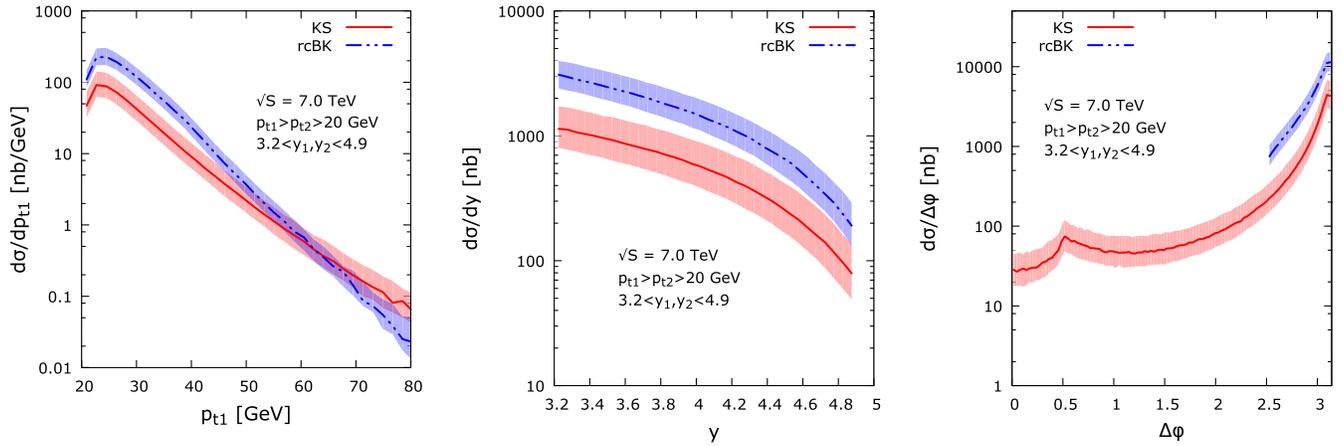
FIG. 1 (color online). Differential cross sections for forward-forward jet productions in p + p collisions, as functions of transverse momentum of the leading jet (left), jet rapidity (middle), and the azimuthal angle between the two hardest jets. The two bands correspond to two different unintegrated gluon distributions used for calculations. The width of the bands comes from varying the renormalization and factorizations scales by factors $\frac{1}{2}$ and 2 around the central value taken as the average p_t of the two leading jets.

distributions in the two scenarios. Here, the difference is mostly in the normalization while the shapes are very similar. The right plot in Fig. 1 shows an observable which is particularly well suited to study saturation, the azimuthal decorrelations between two hardest jets. This observable is nothing else but the azimuthal distance $\Delta\phi = \phi_1 - \phi_2$. If we look at Eq. (2.5), we see that the unintegrated gluon density is taken at the gluon transverse momentum

$$k_{tg}^2 = |\mathbf{p_{t1}} + \mathbf{p_{t2}}|^2 = p_{t1}^2 + p_{t2}^2 + 2p_{t1}p_{t2}\cos\Delta\phi. \quad (4.1)$$

That implies that in the limit $\Delta\phi \to \pi$, which corresponds to almost back-to-back dijet configurations, the gluon is probed at a very low k_t, where saturation is expected to be important. As we see in Fig. 1 (right), the two gluons lead to a somewhat different shape of the decorrelation spectrum above $\Delta\phi \sim 2.5$. We do not plot the rcBK curve below $\Delta\phi \sim 2.5$ since $|\mathbf{p_{t1}} + \mathbf{p_{t2}}|$ is becoming too large compared to the saturation scale where the model does not apply. The peak in the KS result around $\Delta\phi \sim 0.5$ and the rapid decrease below that value come from using the anti-k_t jet algorithm with $R = 0.5$, which leads to significant depletion of the cross section in this region.

The overall conclusion one can draw from the results shown in Fig. 1 is that two different unintegrated gluons, which describe equally well the inclusive F_2 [17,37], can lead to different shapes of the experimentally relevant distributions in the forward-forward dijet production. This may be an indication of the importance of higher order corrections in the evolution of the unintegrated gluon density present in the KS case.

Let us turn to the discussion of possible signatures of saturation. For that we look at the forward-forward dijet production in p + A collisions and compare to the

previously described p + p case. In Figs. 2 and 3, we show the nuclear modification factors defined for each observable $\mathcal{O}$ as

$$R_{pA} = \frac{\frac{d\sigma^{p+A}}{d\mathcal{O}}}{A\frac{d\sigma^{p+p}}{d\mathcal{O}}}. \quad (4.2)$$

If the case of absence of nonlinear effects or in the case in which they are equally strong in the nucleus and in the proton, this ratio equals one. If, however, the nonlinear evolution plays a more important role in the case of the nucleus, the R_{pA} ratio is suppressed below one.

The plots in Fig. 2 show the R_{pA} ratios for the p_t of the leading (left) and subleading (right) jet. In Fig. 3 we have similar ratios for rapidity and azimuthal angle distributions. For each gluon we consider two scenarios to assess possible uncertainties of our prediction. In the rcBK case, we use $d = 2.0$ and $d = 4.0$ [c.f. Eq. (3.4)], while in the KS case, we use $c = 0.5$ and $c = 1.0$ [see formula (3.9)]. As we see in the plots, the scale uncertainty is greatly reduced compared to the distributions shown in Fig. 1. The qualitative behavior of the predictions with two gluons is very similar. They differ mostly at the quantitative level. In particular, in the case of p_t of the leading jet, we observe a suppression of the order of 20%–30% at low p_t for rcBK and 30%–50% for the KS gluon. For the subleading jet this suppression is smaller in both cases. The rapidity R_{pA} ratios are also significantly below one, especially in the very forward region, which corresponds to probing the unintegrated gluon at low x, hence in the domain with strong sensitivity to saturation effects. Finally, in the case of decorrelations, $\Delta\phi$, both gluons lead to up to 60% suppression in the back-to-back limit $\Delta\phi \to \pi$.

To finish, we illustrate in Fig. 4 the impact of saturation effects in the KS evolution by switching off the nonlinear
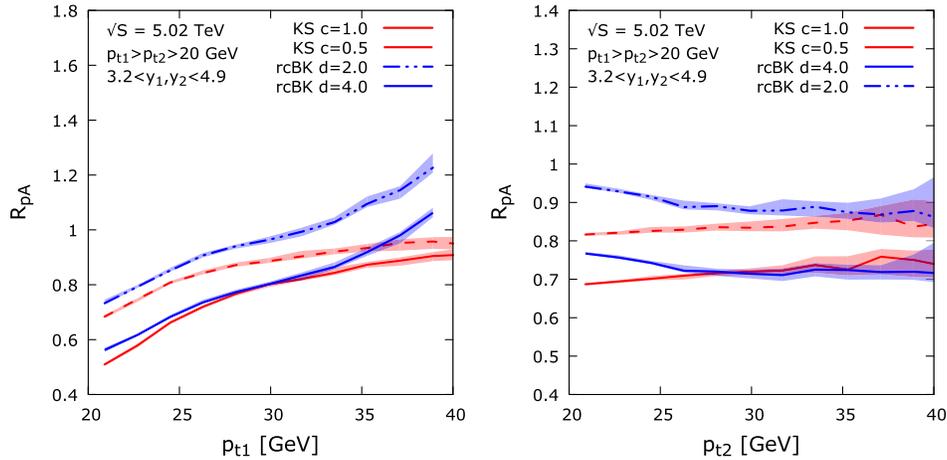
FIG. 2 (color online).   Nuclear modification ratios, defined in Eq. (4.2), as functions of p_ts of the leading (left) and subleading (right) jets produced in the forward region. Different bands correspond to different unintegrated gluon distributions (KS and rcBK) used for calculations. To assess the uncertainty related to the nonlinear effects, the KS result was computed with two values of the c parameter, defined in Eq. (3.9), and the rcBK prediction was obtained with two values of the d parameter from Eq. (3.4). The width of the bands comes from varying the renormalization and factorizations scales by factors $\frac{1}{2}$ and 2 around the central value taken as the average p_t of the two leading jets.
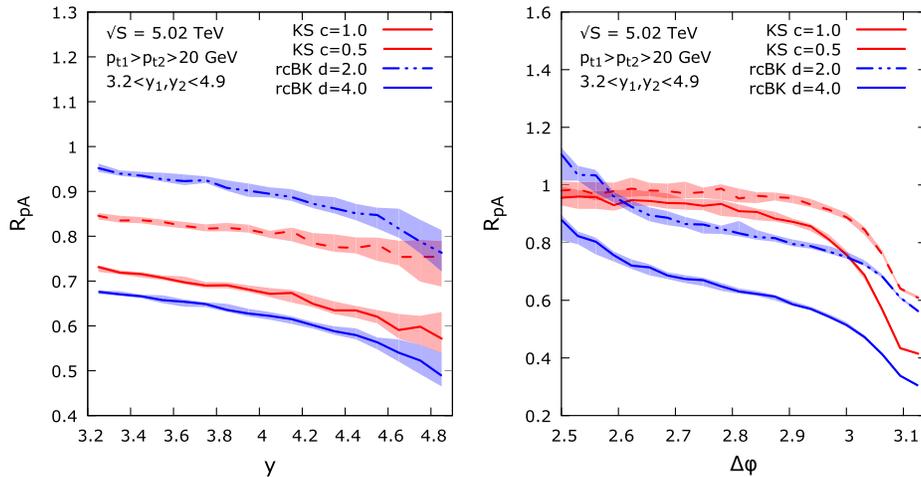
FIG. 3 (color online).   Nuclear modification ratios, defined in Eq. (4.2), as functions of jet rapidity (left) and the azimuthal distance between two hardest jets produced in the forward region (right). All details are as in Fig. 2.

term in the evolution. We note that the parameters of this alternative gluon distribution for the proton, obtained with linear evolution, are readjusted in order to keep a good description of deep inelastic scattering data from HERA. The left plot shows the impact of nonlinear effects on the differential cross section in p + p collisions as a function of the azimuthal angle, and it is large, as expected, near $\Delta \Phi = \pi$. The right plot shows, in the case of the subleading jet p_t dependence, by how much R_{pPb} is reduced if the nuclear gluon density lead is still subject to nonlinear effects, but not a proton one. Of course, with the KS gluon distributions, by construction, if nonlinear evolution is switched off both in the proton and nuclear cases, then $R_{pPb} = 1$.

V. SUMMARY

In this paper, we studied forward-forward dijet production, and we argued that this process is particularly attractive from the low-x point of view. Using the HEF approach [Eq. (2.5)], we provided predictions for distributions and nuclear modification factors in p + Pb vs p + p collisions, as functions of the transverse momenta, rapidities, and relative azimuthal distance of the two hardest jets produced in the forward the region.

Let us first recall that in a small corner of the phase space, for nearly back-to-back di-jets ($|\mathbf{p_{t1}} + \mathbf{p_{t2}}| \leq Q_s$), our calculations should be improved by implementing the more complete factorization formula in Eq. (2.3). Even if
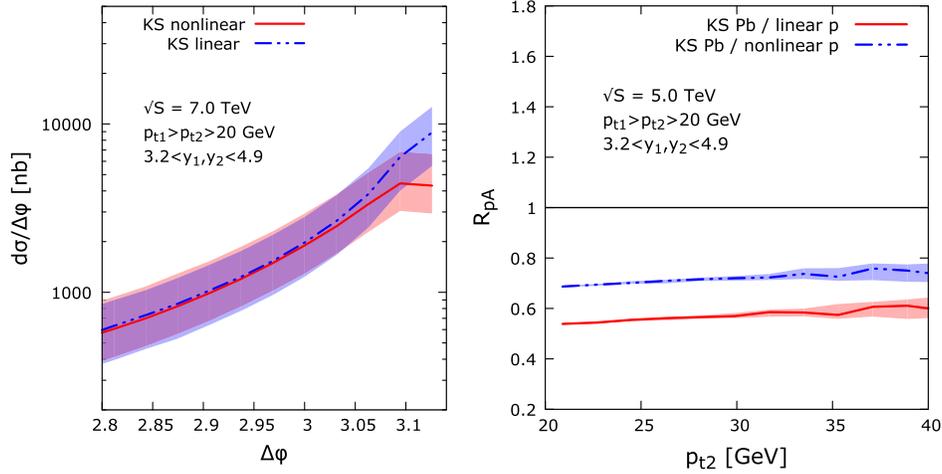
FIG. 4 (color online).   Comparisons of predictions obtained with a linear vs nonlinear proton evolution for the differential cross section in p + p collisions as a function of the azimuthal angle (left) and the nuclear modification factor as a function of p_t of the subleading jet. KS gluon densities are used, with parameter $c = 1$ in the nuclear case.

nonlinear effects are the biggest in there, this small limitation does not affect our conclusions since sizable saturation effects are also seen outside of that kinematic window.

To compute our predictions, we used gluon distributions from two different extensions of the BK equation: the rcBK gluon density obtained from Eq. (3.1) and the KS gluon density obtained from Eq. (3.6). We found that both lead to a very similar behavior of the nuclear modification factors in the domain where the two extensions are applicable. In particular, both sets of predictions suggest significant effects of gluon saturation as one goes from p + p to p + Pb.

Even though it was recently realized that the outcome of high-energy proton-nucleus collisions is quite sensitive to the fact that the nucleon positions in the nucleus fluctuate event by event, so far our R_{pPb} predictions have been obtained using an impact-parameter averaged nuclear saturation scale: Eq. (3.4) in the rcBK case and more indirectly from Eq. (3.9) in the KS case. However, in order to estimate the corresponding uncertainty, we have varied the nuclear saturation strength parameter c (KS) or d (rcBK). A more complete study should certainly include such nucleon-level fluctuation effects; nevertheless, our present results are enough to motivate experimental measurements at the LHC.

Finally, our results also show the importance of higher order corrections to the BK equation. They allow, for example, the extension of the applicability of the unintegrated gluon density toward larger values of transverse momenta, which has consequences for several observables, like the $\Delta\phi$ distribution away from π. In the equations used in this work, those corrections were implemented as educated guesses, but in principle, they deserve a rigorous derivation.

APPENDIX

For convenience, we collect here the matrix elements for the $2 \rightarrow 2$ partonic processes, computed in [12,33,34], and expressed in terms of the transverse momentum and rapidity of the final the state partons. Parametrizing the final state momenta as

$$p_i^\mu = (p_{ti}\cosh y_i, \mathbf{p}_{ti}, p_{ti}\sinh y_i), \qquad i = 1, 2, \quad \text{(A1)}$$

we have

$$\overline{|\mathcal{M}_{qg\rightarrow qg}|^2} = C_1\mathcal{A}_1^{(ab)} + \bar{C}_1\mathcal{A}_1^{(nab)},$$
$$\overline{|\mathcal{M}_{gg\rightarrow q\bar{q}}|^2} = C_2\mathcal{A}_2^{(ab)} + \bar{C}_2\mathcal{A}_2^{(nab)},$$
$$\overline{|\mathcal{M}_{gg\rightarrow g\bar{g}}|^2} = C_3\mathcal{A}_3, \quad \text{(A2)}$$

with the Abelian (ab) and non-Abelian (nab) contributions given by

$$\mathcal{A}_1^{(ab)} = \frac{(K + e^Y)^2((K + e^{-Y})^2 + K^2)}{2K(Ke^Y + 1)(\cosh Y - \cos\phi)}, \quad \text{(A3)}$$

$$\mathcal{A}_1^{(nab)} = 2e^Y(e^Y - \cos\phi)\mathcal{A}_1^{(ab)}, \quad \text{(A4)}$$

$$\mathcal{A}_2^{(ab)} = \frac{(K + e^Y)^2(K^2e^Y + e^{-Y})}{K(Ke^Y + 1)^2}, \tag{A5}$$

$$\mathcal{A}_2^{(nab)} = \frac{\cos\phi}{\cosh Y - \cos\phi}\mathcal{A}_2^{(ab)}, \tag{A6}$$

$$\mathcal{A}_3 = \frac{2(e^{-Y}K + 1)^2(Ke^Y(Ke^Y + 1) + 1)^2(\cos\phi - 2\cosh Y)}{K^2(Ke^Y + 1)^2(\cos\phi - \cosh(Y))}, \tag{A7}$$

where

$$Y = y_1 - y_2, \qquad K = \frac{p_{t1}}{p_{t2}}, \tag{A8}$$

and $C_1 = g^4(N_c^2 - 1)/(2N_c^2)$, $\bar{C}_1 = C_1C_A/(2C_F)$, $C_2 = g^4/(2N_c)$, $\bar{C}_2 = C_2C_A/(2C_F)$, $C_3 = g^4N_c^2/(N_c^2 - 1)$.

[1] L. V. Gribov, E. M. Levin, and M. G. Ryskin, Phys. Rep. **100**, 1 (1983).
[2] F. Gelis, E. Iancu, J. Jalilian-Marian, and R. Venugopalan, Annu. Rev. Nucl. Part. Sci. **60**, 463 (2010).
[3] S. Catani, M. Ciafaloni, and F. Hautmann, Nucl. Phys. **B366**, 135 (1991).
[4] J. L. Albacete and C. Marquet, Phys. Rev. Lett. **105**, 162301 (2010).
[5] A. Stasto, B.-W. Xiao, and F. Yuan, Phys. Lett. B **716**, 430 (2012).
[6] T. Lappi and H. Mantysaari, Nucl. Phys. **A908**, 51 (2013).
[7] C. Marquet, Nucl. Phys. **A796**, 41 (2007).
[8] A. Adare *et al.* (PHENIX Collaboration), Phys. Rev. Lett. **107**, 172301 (2011).
[9] E. Braidot (STAR Collaboration), arXiv:1005.2378.
[10] A. M. Stasto, B.-W. Xiao, and D. Zaslavsky, Phys. Rev. Lett. **112**, 012302 (2014).
[11] Z.-B. Kang, I. Vitev, and H. Xing, arXiv:1403.5221.
[12] M. Deak, F. Hautmann, H. Jung, and K. Kutak, J. High Energy Phys. 09 (2009) 121.
[13] F. Hautmann, Nuovo Cimento C **32N5-6**, 167 (2009).
[14] M. Deak, F. Hautmann, H. Jung, and K. Kutak, arXiv:1012.6037.
[15] M. Deak, F. Hautmann, H. Jung, and K. Kutak, Eur. Phys. J. C **72**, 1982 (2012).
[16] (CMS Collaboration), Report No. CMS-PAS-FWD-10-006.
[17] K. Kutak and S. Sapeta, Phys. Rev. D **86**, 094043 (2012).
[18] A. van Hameren, P. Kotko, and K. Kutak, Phys. Rev. D **88**, 094001 (2013)
[19] I. Balitsky, Nucl. Phys. **B463**, 99 (1996).
[20] Y. V. Kovchegov, Phys. Rev. D **60**, 034008 (1999).
[21] Y. V. Kovchegov and H. Weigert, Nucl. Phys. **A784**, 188 (2007).
[22] I. Balitsky, Phys. Rev. D **75**, 014001 (2007).
[23] J. Kwiecinski, A. D. Martin, and A. M. Stasto, Phys. Rev. D **56**, 3991 (1997).
[24] K. Kutak and J. Kwiecinski, Eur. Phys. J. C **29**, 521 (2003).
[25] A. Dumitru, A. Hayashigaki, and J. Jalilian-Marian, Nucl. Phys. **A765**, 464 (2006).
[26] T. Altinoluk and A. Kovner, Phys. Rev. D **83**, 105004 (2011).
[27] G. A. Chirilli, B.-W. Xiao, and F. Yuan, Phys. Rev. Lett. **108**, 122301 (2012).
[28] G. A. Chirilli, B.-W. Xiao, and F. Yuan, Phys. Rev. D **86**, 054005 (2012).
[29] F. Dominguez, B.-W. Xiao, and F. Yuan, Phys. Rev. Lett. **106**, 022301 (2011).
[30] F. Dominguez, C. Marquet, B.-W. Xiao, and F. Yuan, Phys. Rev. D **83**, 105005 (2011).
[31] A. H. Mueller, B.-W. Xiao, and F. Yuan, Phys. Rev. Lett. **110**, 082301 (2013).
[32] A. H. Mueller, B.-W. Xiao, and F. Yuan, Phys. Rev. D **88**, 114010 (2013).
[33] A. van Hameren, P. Kotko, and K. Kutak, J. High Energy Phys. 12 (2012) 029.
[34] A. van Hameren, P. Kotko, and K. Kutak, J. High Energy Phys. 01 (2013) 078.
[35] E. Iancu and J. Laidet, Nucl. Phys. **A916**, 48 (2013).
[36] J. L. Albacete and Y. V. Kovchegov, Phys. Rev. D **75**, 125021 (2007).
[37] J. L. Albacete, N. Armesto, J. G. Milhano, P. Quiroga-Arias, and C. A. Salgado, Eur. Phys. J. C **71**, 1705 (2011).
[38] F. D. Aaron *et al.* (H1 and ZEUS Collaboration), J. High Energy Phys. 01 (2010) 109.
[39] J. L. Albacete, A. Dumitru, H. Fujii, and Y. Nara, Nucl. Phys. **A897** (2013) 1; the gluon distributions were downloaded from http://faculty.baruch.cuny.edu/naturalscience/physics/dumitru/CGC_IC.html.
[40] N. N. Nikolaev and W. Schafer, Phys. Rev. D **74**, 014023 (2006).
[41] L. N. Lipatov, Sov. J. Nucl. Phys. **23**, 642 (1976); E. A. Kuraev, L. N. Lipatov, and V. S. Fadin, Sov. Phys. JETP **45**, 199 (1977); I. I. Balitsky and L. N. Lipatov, Sov. J. Nucl. Phys. **28**, 822 (1978).
[42] M. Ciafaloni, Nucl. Phys. **B296**, 49 (1988).
[43] S. Catani, F. Fiorani, and G. Marchesini, Nucl. Phys. **B336**, 18 (1990).
[44] S. Catani, F. Fiorani, and G. Marchesini, Phys. Lett. B **234**, 339 (1990).
[45] K. Kutak, K. Golec-Biernat, S. Jadach, and M. Skrzypek, J. High Energy Phys. 02 (2012) 117.
[46] K. Kutak, J. High Energy Phys. 12 (2012) 033.
[47] K. Kutak, arXiv:1206.1223.
[48] M. Deak, J. High Energy Phys. 07 (2013) 087.
[49] K. Kutak and D. Toton, J. High Energy Phys. 11 (2013) 082.
[50] K. Kutak and A. M. Stasto, Eur. Phys. J. C **41**, 343 (2005).

[51] M. Cacciari, G. P. Salam, and G. Soyez, J. High Energy Phys. 04 (2008) 063.

[52] S. Sapeta, FORWARD, the code is available on request from the author.

[53] G. P. Lepage, J. Comput. Phys. **27,** 192 (1978).

[54] G. P. Lepage, CLNS-80/447.

[55] A. van Hameren, arXiv:1003.4953.

[56] A. van Hameren, Acta Phys. Pol. B **40,** 3119 (2009).

[57] P. Kotko, LXJET, the code is available at http://annapurna.ifj .edu.pl/~pkotko/LxJet.html.

[58] S. Jadach, Comput. Phys. Commun. **152,** 55 (2003).

[59] H. -L. Lai, M. Guzzi, J. Huston, Z. Li, P. M. Nadolsky, J. Pumplin, and C.-P. Yuan, Phys. Rev. D **82,** 074024 (2010).